

Cold Sprayed MCrAlY as a Bondcoat Candidate for TBC Application

X. Ma and P. Ruggiero

Curtiss-Wright Corporation, Surface Technologies Division, East Windsor, CT, USA

Abstract

As an emerging technique, cold gas dynamic spray is one of the latest tools for dimensional repair and coating applications. Cold spray (CS) utilizes high velocity particles as feedstock rather than high temperature to produce a coating without over melting feedstock, and thereby achieves a free-oxide coating. One of today's critical coating applications is thermal barrier coating (TBC) for high efficiency turbine engine components, assisting and enabling today's super alloys for turbine components to operate at a higher firing temperature. Many studies reveal that the formation of thermally grown oxide (TGO) on MCrAlY bondcoat, and the surface morphology profile of the bondcoat play paramount roles in failure modes and lifetimes of TBCs. This work has been focused on exploring the feasibility of CS MCrAlY as a bondcoat candidate for TBC application by comparing with those deposited by thermal spray processes, mainly plasma spray (APS) and high velocity oxygen fuel (HVOF).

In this work, the features and properties of CS coatings were characterized mainly on microstructure, surface morphology, and TGO formation in isothermal oxidation test at 1100°C. Also, CS bondcoat and its thermal barrier coating were tested together with APS and HVOF formed TBC coatings. CS NiCoCrAlY coatings are identified with some unique aspects and characteristics: A desirable microstructure can be achieved, with oxide-free and high density. Solid solution of NiAl phase at local regions of grain boundaries is discovered; CS-bondcoat has a honeycomb network-like surface morphology. Long-range roughness is characterized from all honeycomb networks, and short-range roughness from the peaks within individual network cells; Kinetic curve of isothermal oxidation test at 1100°C indicates that a low-rate and stable TGO scale is formed on CS-bondcoat; and thermal cycling test demonstrates that CS-bondcoat TBC and APS-TBC have higher resistance to the spallation of ceramic topcoat.

Introduction

Cold gas dynamic spray, also so-called supersonic particle cold deposition, is one of the latest methods to restore the dimensional and or structural damaged structures for a recent decade. In CS process, a solid-state coating is applied by exposing a substrate to a high velocity (300–1200 m/s) flux of particles accelerated by a supersonic jet of

compressed gas at a temperature that is always lower than the melting point of the feedstock material [1-3]. As a consequence, the deleterious effects of high-temperature oxidation, evaporation, melting, crystallization, residual stresses, and other common problems for traditional thermal spray methods are minimized or eliminated. Therefore, CS is suitable for the deposition of oxygen-sensitive materials such as aluminum, copper, or titanium; temperature and sensitive materials as glass and polymer substrates, nanostructured and amorphous powders; or oxidation sensitive materials such as MCrAlY bondcoat in a thermal barrier coating [4-7].

Thermal barrier coatings (TBCs) are highly advanced surface engineering systems usually applied to superalloy surfaces, such as land-based gas turbine or aero-engine parts operating at elevated temperatures [8-12]. These coatings serve to insulate components from large and prolonged heat loads by utilizing thermally insulating and oxidation resistance of TBC materials. These coating systems typically consist of a metallic bondcoat and a ceramic topcoat, which can sustain an appreciable temperature difference between the load-bearing alloy substrate and the coating surface. TBCs allow for higher operating temperatures, and extend part life by reducing oxidation and thermal fatigue.

Many investigations have indicated that TBC failure is ultimately connected to the large residual compression in the thermal grown oxide (TGO) scale through its roles in amplifying imperfections near the interfaces of bondcoat, TGO and topcoat, and to the stress associated with crack initiation and propagation around the peaks of bondcoat roughness profile [13-15]. Volumetric strains due to TGO developed during breakaway oxidation can result in formation of significant out-of-plane tensile stresses within the ceramic topcoat. These stresses are located along the flanks of the bondcoat protuberances in locations where sub-critical cracks initiate. The magnitude of the stresses increases with bond coat surface roughness, after the initiation of breakaway oxidation and after cooling. Therefore, further improvement of TBC systems should consider such key characteristics, including TGO behavior and morphology profile of the bondcoat.

The objective of this study is to explore a new TBC system with a unique bondcoat applied by latest CS technology, which is capable of producing an oxide-free deposit with enhanced surface morphology compared to thermal sprayed bondcoats. With particular interest on the influence of bondcoat roughness and TGO layer on TBC failure

mechanisms. TBC specimens incorporated with a CS bondcoat are tested in isothermal oxidation condition to evaluate TGO kinetics, and thermally cyclic testing to examine the spallation resistance of the ceramic layer. This work aims to provide better understanding of high temperature behavior of CS bondcoat and its TBC/ceramic layer, and comparative performance in simulated oxidation environments. Preliminary test results exhibit CS as a potential process to apply a superior bondcoat for the improvement of engineered TBCs.

Experimental

Powder Materials

NiCoCrAlY powders used have the same chemistry but different particle sizes, for CS and the thermal spray trials as listed in **Table 1**. The powders are manufactured by induction melting raw materials in an inert gas atmosphere followed by atomization using N₂ gas, and have a typical spherical morphology with good flowability as a feedstock. The fine-sized powder (Type-A) is used for CS, as well as HVOF. The coarse-sized powder Type-B is used for APS. The cross-sections of the two-version powders are observed in **Figure 1**. Typically, phase distribution in a NiCoCrAlY material is observed to be the dispersion of β-NiAl, γ'-Ni₃Al and α-Cr in primary matrix of γ-NiCo. A plasma-densified ZrO₂-8%Y₂O₃ powder was used for the topcoat of all TBC specimens applied by APS.

Table 1 Powders and particle sizes used for coating trials

Type	D10	D50	D90
Powder-A	18 μm	32 μm	38 μm
Powder-B	40 μm	58 μm	88 μm

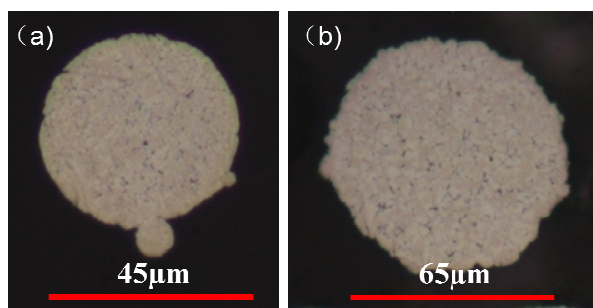


Figure 1: Cross-section views of NiCoCrAlY powders used for CS and thermal spray trials. (a) Type-A; (b) Type-B.

Spray Setup

In this work, CS coatings were prepared by utilizing a commercial CS system. A de Laval nozzle and upstream powder injection is equipped with the system, in which N₂ gas at elevated pressure is introduced to a heater and powder feeding vessel. The high pressure and high temperature N₂ gas is taken into the converging/diverging nozzle to generate a supersonic flow. The system incorporates pressure and temperature probes in the main gas chamber. The substrates

were grit blasted and subjected to ultrasonic cleaning prior to the coating deposition. To optimize the CS parameter, the chamber pressure was varied over the range 4.1-4.8 MPa and gas preheat temperature from 705-870°C. The CS process was then optimized in terms of stagnation pressure and gas preheat temperature on the basis of coating density and deposition efficiency. **Table 2** provides the optimized process parameters for CS bondcoat. Coatings were deposited onto substrates of superalloy IN718.

Table 2 Experimental conditions for CS of MCrAlY

Main Gas Pressure	Pre-Heat Temperature	Chamber Temperature
4.8 MPa	870 °C	815 °C

Comparison specimens were prepared by employing commercial thermal spray systems. APS and HVOF coatings were sprayed with a F4-gun system and Jetkote-gun system separately, using proprietary spray conditions, which can produce coatings with acceptable microstructures and thickness for typical TBC applications.

Coating Characterization

CS and thermal-sprayed coatings were observed on surface morphologies using scanning electron microscope (SEM) and laser confocal scanning microscope (LCSM). 2D and 3D surface roughness was measured using profilometer and laser confocal microscope, and then surface roughness such as Ra was determined for those bondcoats. Coating specimens were sectioned in a direction perpendicular to the coating plane and then metallographic specimens were prepared using a standardized grinding and polishing procedure. The cross-sections of metallographic specimens were examined using SEM and an optical microscope. In conjunction with image analysis software, microstructure, porosity and oxide levels of the coatings were estimated.

Coating specimens after oxidation tests also were characterized. Phase compositions of TGOs formed on bondcoats were analyzed using X-ray diffraction (XRD). Morphologies of TGOs were observed using SEM and LCSM. Chemical compositions of oxidized bondcoats were examined using SEM/EDAX technique. TBC specimens after oxidation testing were inspected using a digital microscope to obtain the details in failed coating locations.

Coating Testing

Isothermal oxidation test of CS, APS and HVOF-formed bondcoats without a topcoat was conducted in air at 1100 °C. First, bondcoat test specimens with smooth surface finish (Ra<0.8 μm) were prepared by grinding and polishing. Then, the test specimens were placed in individual Al₂O₃ crucibles which were located sequentially in the flat-temperature zone of a Muffle furnace with a temperature accuracy of +/-15°C. At an interval of 5 to 20 hours, the weight changes of test specimens were measured as to determine oxidation kinetics.

Thermal cycling test of all TBC specimens was performed in air by rapid cooling from heating temperature of 1050°C to near room temperature. Prior to thermal cycling test, TBC

specimens were pre-oxidized in a box furnace at 1100°C for 50 hours to form TGO scales between bondcoat and topcoat. For one thermal cycle, test specimens were heated at 1050°C for about 30 minutes, then were removed from the furnace and rapidly quenched into a water container. After cooling to water temperature about 25 to 35°C, test specimens were taken from the container and dried with a hot air blower. After examined on TBC surfaces for any damage or failure under a digital microscope, test specimens were put back to the furnace to continue thermal cycling test.

On the completion of total 100 cycles, test specimens were evaluated based on the integrity or failure of TBCs, especially topcoats. The cooling rate of thermal cyclic test was measured using attached thermal couple, and temperature profile as shown in **Figure 2**. Obviously, the samples have much high cooling rate with water compared to conventional air cooling.

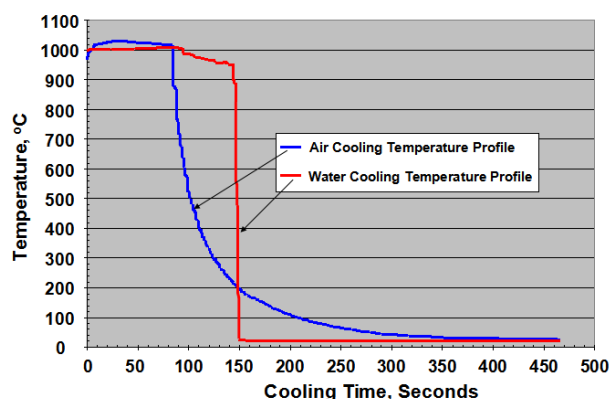


Figure 2: Temperature profile for thermal cycling test by rapidly cooling from 1050 to 25-35 °C in water.

Results and Discussion

Morphologies of Bondcoats

Morphologies and surface roughness Ra of bondcoats applied by CS, APS and HVOF are compared in **Figure 3**. CS-bondcoat shows a honeycomb-like peak-valley surface. Within each “honeycomb cell”, some peak-valley feature also is observed, which is similar to the cases of APS and HVOF coatings where mountain-like surface features are typical. The unique morphology of CS-bondcoat can be characterized by a long-range roughness measured across all networked honeycomb areas and a short-range roughness measured within individual honeycomb.

Overall long-range roughness Ra for CS-bondcoat is about 12.9µm, and short-range roughness Ra is about 7.5µm. The long-range Ra 12.9µm of CS-bondcoat is close to the Ra 12.5µm of APS-bondcoat, and the short-range Ra is slightly higher than the Ra 5.6µm for HVOF-bondcoat. By eliminating those sharp peaks that typically appeared on APS-bondcoat, the networked peaks with CS-bondcoat may be desirable for lowering residual stress in a TBC related to bondcoat protuberances in the locations where sub-critical

cracks initiate as indicated in some TBC studies [16, 17]. Meanwhile, short-range roughness provides local locking points for topcoat to enhance coating adhesion. The formation of the unique surface profile with CS-formed bondcoat can be explained mostly by the formation mechanism of CS coating due to severe deformation and stockpile of unmelted particles [18], and partially by the spray conditions applied.

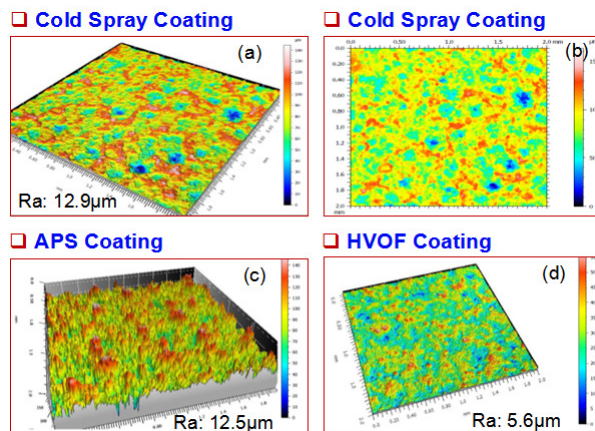


Figure 3: Morphologies of bondcoats applied by CS (a, b), air plasma spray (c) and HVOF spray (d).

Microstructures

Cross-section views of microstructures of as-sprayed bondcoats are shown in **Figure 4**. CS-formed bondcoat (Fig. 4a) shows a clean oxide-free microstructure. Porosity of about 1-2% is identified using image analysis. Bondcoat/

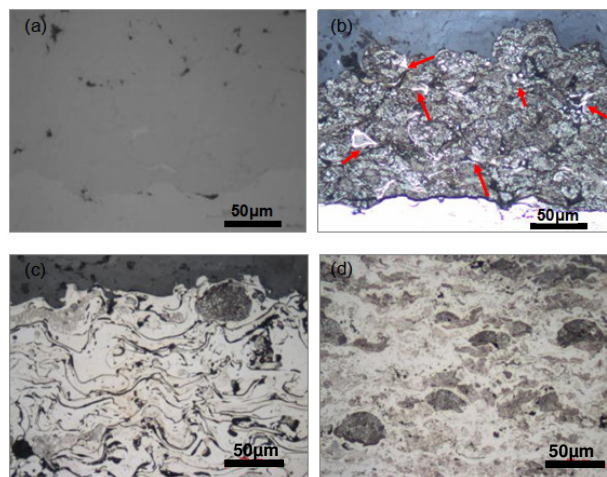


Figure 4: Microstructures of MCrAlY bondcoats applied by CS (a: as-sprayed; b: etched), air plasma spray (c: etched) and HVOF spray (d: etched).

substrate interface is well bonded. To unveil more details of microstructures and phase distributions, coatings were chemical etched. As shown in **Figure 4c** and **4d**, the majority of APS and HVOF-formed MCrAlY coating is white-colored, with exception of small dark areas in the white matrix. The white coating matrix is due to the

formation of metastable microstructure after fully melting of coating material. The dark areas are due to the retaining of original feedstock material without melting or partially melting of particles. In contrast, CS-formed coating shown in **Figure 4b** retains the microstructure of feedstock without melting and associated phase solutioning. However, with a surprise and great interest, some dispersive white phases are observed along grain boundaries as the arrows indicated. The formation of white soluble phases may be explained by phase transformation and amorphization of alloy during CS process, induced by remarkable plastic deformation due to high-velocity impact of particles. Non-uniform strain and temperature distribution near the grain boundary or interface regions was reported in CS-coating [19]. In addition, temperature rise observed at the highly deformed interface region appears with a distribution similar to that of the effective plastic strain, which will promote phase solution in the local regions. Moreover, the effective plastic strain and temperature rise are dependent on the particle velocity and the initial particle temperature. High degree deformation enhanced by adiabatic shear effect leads to the formation of metal jetting. It is believed the existence of soluble or metastable phases along grain boundaries in a CS-coating will be helpful to strengthen the boundaries and thus contribute to the increase in coating cohesion strength and integrity. The microstructures of thermal barrier coatings used in thermal cycling test are shown in **Figure 5**. It is noticed that the interfaces of bondcoat/topcoat in CS- and APS-TBCs are much rougher than in HVOF-TBC.

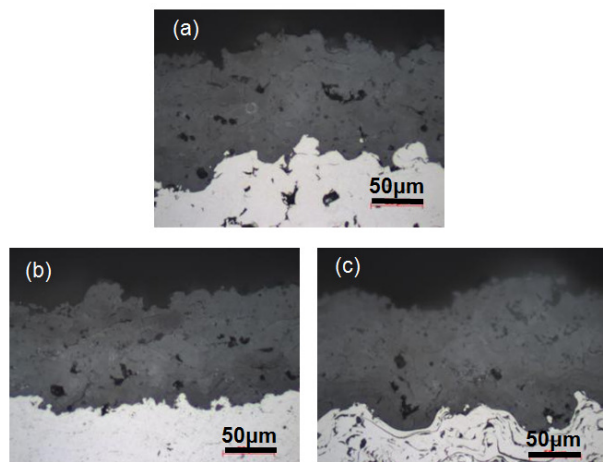


Figure 5: Microstructures of thermal barrier coatings with different types of bondcoats. (a) Cold-sprayed bondcoat, (b) APS-sprayed bondcoat, and (c) HVOF-sprayed bondcoat.

Isothermal TGO Kinetics

Three bondcoats were oxidized at 1100°C for 100 hours in air, and their mass gains during the high temperature dwells are plotted in **Figure 6a**. It is clear that mass gains are much lower for CS and HVOF-formed bondcoats than for APS-formed bondcoat. Based on these mass gains, the oxidation constants K_p are calculated using a complete parabolic law fitting procedure. The K_p constant is $8.65 \times 10^{-12} \text{ g}^2/\text{mm}^4 \cdot \text{hr}$ for CS-bondcoat, $9.26 \times 10^{-12} \text{ g}^2/\text{mm}^4 \cdot \text{hr}$ for HVOF-bondcoat, and $56.1 \times 10^{-12} \text{ g}^2/\text{mm}^4 \cdot \text{hr}$ for APS-bondcoat, respectively.

In the case that the experimental data deviate from true parabolic law, the calculated K_p values may not be wholly true for some coatings, especially for APS-bondcoat and CS-bondcoat during the transition period or quasi-steady-state stage of oxidation for the first 20-30 hours. In a similar study of thermal exposure, it was observed that TGO exhibited a three-stage growth behavior on APS-CoNiCrAlY, whereas on HVOF and CS-CoNiCrAlYs, the growth of TGOs showed an instantaneous growth followed by a parabolic growth [20]. CS-bondcoat demonstrates a low and stable oxidation rate during the test period, and this result can be explained based on two main factors: (i) CS-bondcoat is oxide-free due to the nature of CS without melting of feedstock. Thus, there no depletion of those elements (such as Al, Cr and Y) for promoting the formation of α -alumina in the early stage of oxidation [21]. (ii) Sub-structured and/or finer grains are introduced into CS-bondcoat during the CS process by supersonic velocity impact with high energy. As indicated in studies of milled or nanocrystalline MCrAlY coatings, finer grained MCrAlY can affect the outward diffusion of elements such as Al in the bondcoat to coating surface, which ultimately promotes stable and homogeneous TGO growth [22-24].

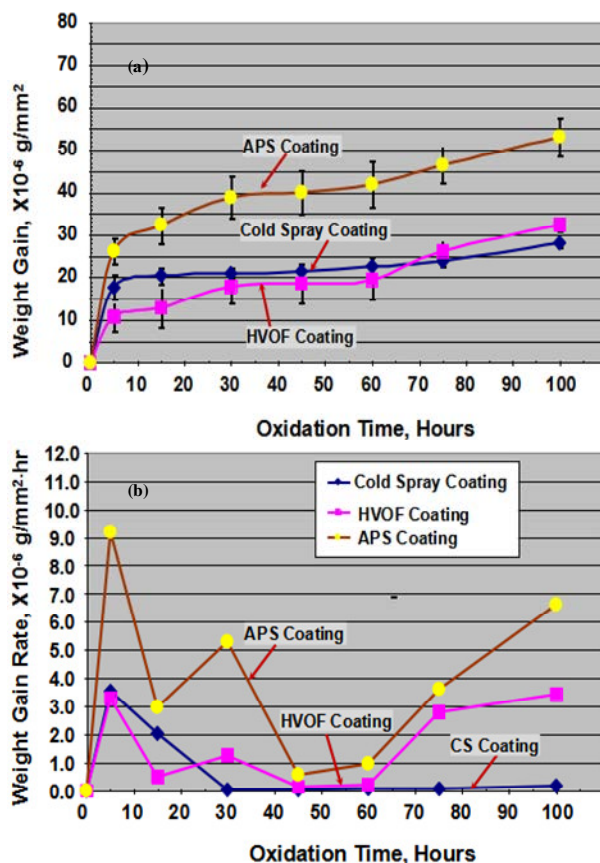


Figure 6: Plots of weight gain vs time (a) and plots of weight gain rate vs time (b) for MCrAlY bondcoats tested in isothermal oxidation at 1100 °C.

To better describe TGO growth and stability, weight gaining rates versus time also are plotted in **Figure 6b**. It is obvious that TGO is formed rapidly on those bondcoated during

transition period of 0 to 5 hours. Then TGO growth slows down and becomes stable. TGO on CS-bondcoat has a very slow growth rate during the period of test, but TGO on APS or HVOF bondcoat shows several stages of fast growth of TGO, such as after thermal exposure of 60 hours. The TGO scales increase dramatically in weight should be related to the formation of non-alumina TGO such as Ni(Cr, Al)₂O₄ spinel or re-healing of TGO if any cracking or spallation happens in existing TGO layer [25].

TGO Morphology

Morphologies of TGO scales grown on oxidized bondcoats were observed with SEM and laser scanning microscope. As shown in **Figure 7**, CS-bondcoat has a homogenous TGO film, only a few small peaks of fast-growth TGO are identified on the surface. For comparison, APS-bondcoat forms a TGO scale with distinct areas for slow-growth TGO and fast-growth TGO. It is believed that TGO scales consist primarily of α -Al₂O₃ in both slow- and fast-growth areas, and slow-growth area without the presence of detrimental fast-growing mixed oxides, but a fast-growth area with a limited presence of other oxides such as Ni(Cr,Al)₂O₄ spinel. In addition, localized Al depletion near top surface of bondcoat can also nucleate a fast-growing non-protective TGO on APS-bondcoat [26].

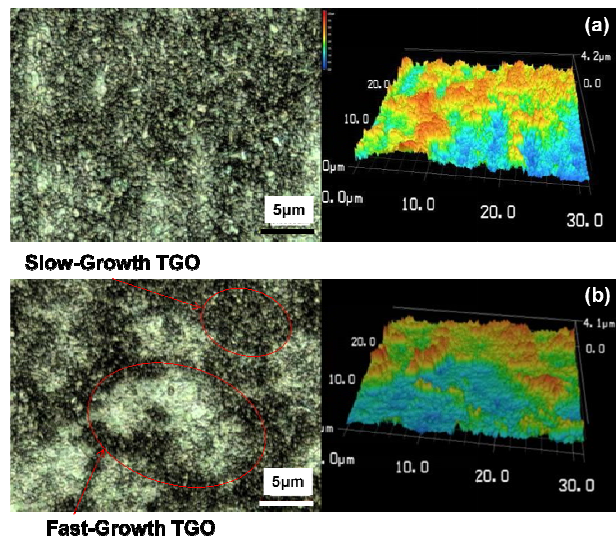


Figure 7: 2D and 3D Morphologies of TGO scales formed on the bondcoats after oxidation exposure at 1100 °C for 100 hours, (a) CS-bondcoat, (b) APS-bondcoat.

TGO Phase Analysis

XRD analysis results of bondcoats after 100-hour oxidation test at 1100°C are shown in **Figure 8**. On CS-bondcoat sample, primary α -Al₂O₃ phase is identified. On APS and HVOF-bondcoat samples, similar XRD results are verified. It is assumed that there are generally limited amount of mixed oxide phases, such as NiO and or spinel phase in TGO scales [27], but these are not well detected by XRD method.

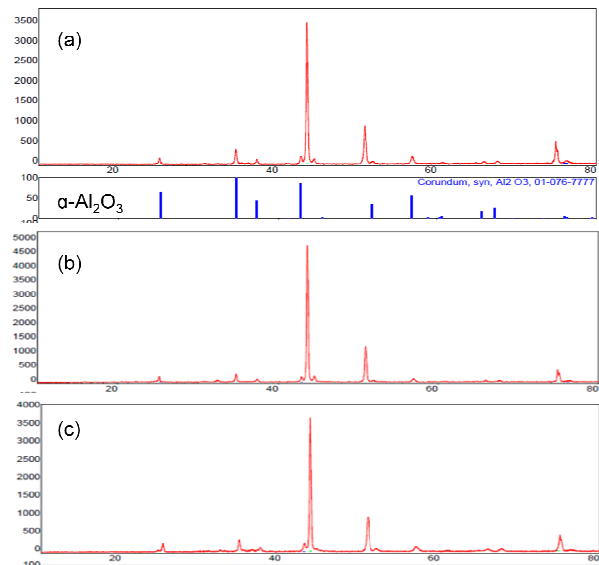


Figure 8: XRD analysis results of TGO scales formed on the bondcoats after oxidation test at 1100 °C for 100 hours. (a) CS-bondcoat, (b) HVOF-bondcoat, and (c) APS-bondcoat.

Microstructure of Oxidized Bondcoat

After isothermal oxidation test at 1100 °C for 100 hours, microstructures of bondcoats were examined and are shown in **Figure 9**. Meanwhile, the depletion zones of Al are observed by SEM and their chemicals are analyzed by EDAX, in the vicinity of underneath bondcoats of TGO scales. In the microstructures the depleted zones can be clearly identified, where there is much less dispersive NiAl phase. The depths of the depletion zones are measured as

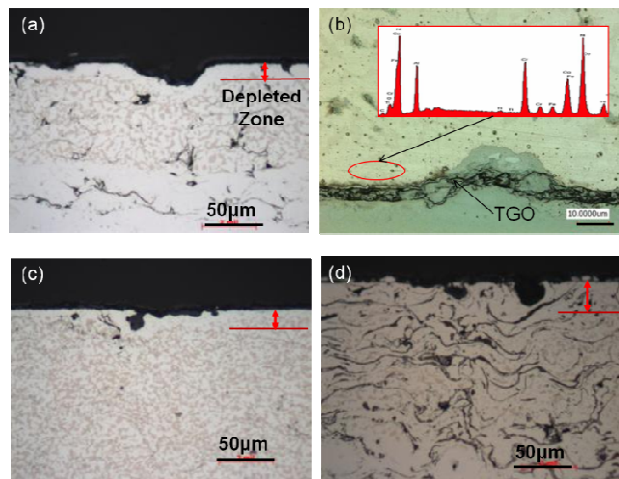


Figure 9: Optical microstructures of the bondcoats after oxidation test at 1100 °C for 100 hours. (a) CS-bondcoat, (b) CS-bondcoat, SEM image and EDAX analysis, (c) HVOF-bondcoat, and (d) APS-bondcoat.

about 20 µm in CS- and HVOF-bondcoats, and about 40 µm in APS-bondcoat. The large depletion zone in APS-bondcoat

can be interpreted by the outward diffusion of Al in β -NiAl phase and more Al consumption to form TGO scale at a higher oxidation growth rate. In the depletion zone of CS-bondcoat, SEM/EDAX analysis verifies that average Al content is reduced from original 10.5 - 11 wt.% to 8.5 - 9.0wt.%. This level of Al content should be still sufficient to supply Al for continuous and stable growth of primary α -Al₂O₃ scale [28].

Thermal Cyclic Results

Test specimens were inspected to determine coating damages and failure locations after cooling down to room temperature for each thermal cycle. The initiation of topcoat spallation damage on the coating edge exists at the 20th cycle on HVOF-bondcoated TBC, and at the 60th cycle on CS-bondcoated TBC. APS-bondcoated TBC shows no coating failure during the test period of total 100 cycles. As shown in **Figure 10**, the topcoat over CS-bondcoat spalls in two local areas (about 10% of total surface area) near specimen's edge. In the worst failure case of HVOF-bondcoated TBC, topcoat spalls around specimen's edge, with spallation area about 25% of total surface area. From the observation on morphologies of failed topcoats, it seems that the failure starts with cracking inside topcoats, and ends with spallation of topcoats at TGO/topcoat interface. The test results may be mostly correlated to the surface roughness of bondcoats, rather than TGO growth rates under the aggressive and rapid cooling test condition.

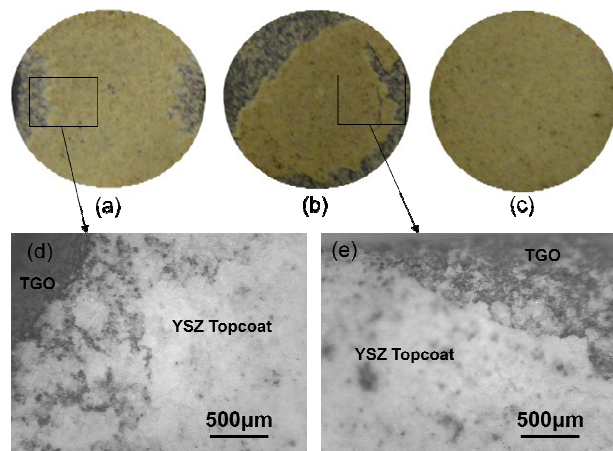


Figure 10: Surface views of TBC specimens after thermal cycling oxidation test at 1050 °C for 100 cycles. (a, d) CS-bondcoat, (b, e) HVOF-bondcoat, and (c) APS-bondcoat.

Conclusions

In this work, a NiCoCrAlY bondcoat was deposited by CS process. Coating features and properties were characterized mainly on microstructure, surface morphology, and TGO formation in isothermal oxidation test at 1100°C. In addition, thermal barrier coating incorporated with the CS bondcoat was evaluated in thermal cycling test. Meanwhile, CS bondcoat and its thermal barrier coating were tested together with APS and HVOF formed coatings, and their properties and performance were compared. From the present work, CS

coatings are identified with some unique aspects and characteristics:

- (1) A desirable microstructure can be achieved with CS-NiCoCrAlY bondcoat, with oxide-free and high density. Without melting the original feedstock during CS process, phase and structure in feedstock is retained mostly. But solid solution of NiAl phase at local regions of grain boundaries is observed.
- (2) CS-bondcoat has a honeycomb network-like surface morphology compare to mountain peak-like ones with HVOF and APS-bondcoats. Long-range roughness is characterized from all honeycomb networks, and short-range roughness from the peaks within individual network cells. Overall long-range roughness of CS bondcoat is similar to that of APS-formed bondcoat, and short-range roughness is slightly higher than HVOF-formed bondcoat.
- (3) Kinetic curve of isothermal oxidation test at 1100 °C indicates that a low-rate and stable TGO scale is formed on CS-bondcoat. XRD analysis confirms that the TGO scale consists of primary α -Al₂O₃ oxide, with minor mixed oxides. At the early stage of transitional oxidation, kinetic of CS-bondcoat deviates from parabolic law at a high oxidation rate, and then follow well the parabolic law after a stable oxide scale is formed with increasing oxidation time.
- (4) In consistent with the oxidation kinetic, the depletion zones in CS and HVOF-bondcoats are much small compared to that in APS-bondcoat. The results indicate that the consumption of Al sources in the bondcoats is much less due to rich Al sources in oxide-free bondcoats and the formation of low-growth TGO scales.
- (5) Thermal cycling test demonstrates that CS-bondcoated TBC and APS-TBC have higher resistance to the spallation of ceramic topcoat. HVOF-bondcoated TBC shows early failure of topcoat. It is concluded that TBC's failure is correlated predominantly to the surface roughness of those bondcoats, rather than TGO growth rates.

References

- [1] Papyrin, A. *et al.*, Cold Spray Technology, Elsevier (2006), pp. 1-336.
- [2] Champagne, V. K., The Cold Spray Materials Deposition Process, Woodhead (2007), pp. 1-362.
- [3] Champagne, V. K., "The Repair of Magnesium Rotorcraft Components by Cold Spray: Cold Spray-Al," *Journal of Failure Analysis and Prevention*, Vol. 8, No. 2 (2008), pp. 164-175.
- [4] Zahiri, S. H. *et al.*, "Recrystallization of Cold Spray-Fabricated CP Titanium Structures," *Journal of Thermal Spray Technology*, Vol. 18, No. 1 (2009), pp. 16-22.

- [5] Zaikovskii, V. N. *et al.*, “Control of Spray Spot Shape in Cold Spray Technology,” *Thermophysics and Aeromechanics*, Vol. 21, No. 2 (2014), pp. 223-230.
- [6] Cavaliere, P. *et al.*, “Processing Conditions Affecting Grain Size and Mechanical Properties in Nanocomposites Produced via Cold Spray,” *Journal of Thermal Spray Technology*, Vol. 23, No. 7 (2014), pp. 1089-1096.
- [7] Kim, D. *et al.*, “Cold Spray Deposition of Copper Electrodes on Silicon and Glass Substrates,” *Journal of Thermal Spray Technology*, Vol. 22, No. 7 (2013), pp. 1092-1102.
- [8] Padture, N. P. *et al.*, “Thermal Barrier Coatings for Gas-Turbine Engine Applications,” *Science*, Vol. 296, No. 5566 (2002), pp. 280-284.
- [9] Zhu, D. *et al.*, “Sintering and Creep Behavior of Plasma Sprayed Zirconia and Hafnia-Based Thermal Barrier Coatings,” *Surface and Coating Technology*, Vol. 108-109 (1998), pp.114-120.
- [10] Clarke, D. R. *et al.*, “Thermal-Barrier Coating for More Efficient Gas-Turbine Engines,” *MRS Bulletin*, Vol. 37 (2012), pp. 891-898.
- [11] Goward, G. W., “Progress in Coatings for Gas Turbine Airfoils,” *Surface and Coatings Technology*, Vol.108-109 (1998), pp. 73-79.
- [12] Beele, W. *et al.*, “The Evolution of Thermal Barrier Coatings — Status and Upcoming Solutions for Today’s Key Issues,” *Surface and Coatings Technology*, Vol.120-121 (1999), pp. 61-67.
- [13] Evans, A. G. *et al.*, “Mechanisms Controlling the Durability of Thermal Barrier Coatings,” *Progress in Materials Science*, Vol. 46 (2001), pp. 505-553.
- [14] Busso, E. P. *et al.*, “Effects of Breakaway Oxidation on Local Stresses in Thermal Barrier Coatings,” *Acta Materialia*, Vol. 58 (2010), pp. 1242-1251.
- [15] Bolcavage, A. *et al.*, “Thermal Shock Testing of Thermal Barrier Coating/Bondcoat Systems,” *Journal of Materials Engineering and Performance*, Vol.13, No. 4 (2004), pp. 389-396.
- [16] Schlichting, K. W. *et al.*, “Failure Modes in Plasma-Sprayed Thermal Barrier Coatings,” *Mater.Sci. Eng. A*, Vol. 342 (2003), pp. 120-130.
- [17] Gupta, M. *et al.*, “Influence of Topcoat-Bondcoat Interface Roughness on Stresses and Lifetime in Thermal Barrier Coatings,” *Journal of Thermal Spray Technology*, Vol. 23, No. 1-2 (2014), pp. 170-181.
- [18] Assadi, H. *et al.*, “Bonding Mechanism in Cold Gas Spraying,” *Acta Materialia*, Vol. 51, No. 15 (2003), pp. 4379-4394.
- [19] Luo, X. *et al.*, “High Velocity Impact Induced Microstructure Evolution during Deposition of Cold Spray Coatings: A Review,” *Surface and Coatings Technology*, Vol. 254 (2014), pp. 11–20.
- [20] Chen, W. R. *et al.*, “The Oxidation Behavior of TBC with Cold Spray CoNiCrAlY Bond Coat,” *Journal of Thermal Spray Technology*, Vol. 20, No. 1-2 (2011), pp. 132-138.
- [21] Yuan, F. H. *et al.*, “Oxidation Behavior of Thermal Barrier Coatings with HVOF and Detonation-Sprayed NiCrAlY Bondcoats,” *Corrosion Science*, Vol. 50, No. 6 (2008) , pp. 1608–1617.
- [22] Ma. X. *et al.*, “Innovation of Ultrafine Structured Alloy Coatings Having Superior Mechanical Properties and High Temperature Corrosion Resistance,” *Journal of Thermal Spray Technology*, Vol. 17, No. 5-6 (2008), pp. 933-941.
- [23] Ma, K. *et al.*, “Isothermal Oxidation Behavior of Cryomilled NiCrAlY Bond Coat: Homogeneity and Growth Rate of TGO,” *Surface and Coatings Technology*, Vol. 205, No. 21–22 (2011), pp. 5178–5185.
- [24] Ajdelsztajn, L. *et al.*, “Oxidation Behavior of HVOF Sprayed Nanocrystalline NiCrAlY Powder,” *Materials Science and Engineering: A*, Vol. 338, No. 1–2 (2002), pp. 33–43.
- [25] Richer, P. *et al.*, “Oxidation Behaviour of CoNiCrAlY Bond Coats Produced by Plasma, HVOF and Cold Gas Dynamic Spraying,” *Surface and Coatings Technology*, Vol. 204, No. 24 (2010), pp. 3962–3974.
- [26] Evans, H. E., “Oxidation Failure of TBC Systems: An Assessment of Mechanisms,” *Surface and Coatings Technology*, Vol. 206, No. 7 (2011), pp. 1512–1521.
- [27] Seo, D. *et al.*, “Comparative Study on Oxidation Behavior of Selected MCrAlY Coatings by Elemental Concentration Profile Analysis,” *Applied Surface Science*, Vol. 255, No. 5 (2008), pp. 2581–2590.
- [28] Eriksson, R. *et al.*, “MCrAlY Coating Design Based on Oxidation–Diffusion Modelling. Part II: Lifing Aspects,” *Surface and Coatings Technol.*, Vol. 253 (2014), pp. 27–37.